Chapter 16
Substructuring of a Nonlinear Beam Using a Modal Iwan Framework, Part II: Nonlinear Modal Substructuring

Daniel Roettgen, Matthew S. Allen, Daniel Kammer, and Randall L. Mayes

Abstract In a companion paper (Roettgen, D.R., et al.: Substructuring of a nonlinear beam using modal Iwan framework, Part 1: nonlinear modal model identification. Presented at the international modal analysis conference XXXV, Garden Grove, 2017), "Substructuring of a nonlinear beam using modal Iwan framework, Part I: Nonlinear Modal Model Identification", nonlinear modal models are constructed for an experimental substructure that represent the dynamics using a set of uncoupled weakly nonlinear modes. This assumes that the linear modes of the structure remain uncoupled so that the nonlinearity can be described in a mode by mode fashion. These nonlinear modal models can be used to simulate the response of the experimental system. This paper demonstrates the use of these models to represent a substructure in an experimental-analytical substructuring prediction. The authors utilize the transmission simulator method on the experimentally derived models to generate predictions of a modified Brake-Reuss Beam system. The substructuring predictions are then compared to a truth test data set to validate the method. To further understand the limitations of the method and its sensitivity to measurement noise, the modal substructuring approach is also simulated on a finite element model of the beam that contains three discrete nonlinear elements to represent the joint.

Keywords Experimental Nonlinear Substructuring • Modal Iwan Models • Transmission Simulator Method

16.1 Introduction

Experimental-analytical substructuring allows one to predict the dynamic response of an assembly by coupling substructures derived from experiments with substructures represented by finite element models. There are numerous applications of experimental-analytical substructuring, but in particular this is useful when one part of a system is difficult to model. When building a structure from several subcomponents, there are often many joints involved, either contained within one subcomponent or between them. Such joints are known to be a significant source of nonlinear damping in built-up assemblies, and their stiffness is difficult to predict when modeling. One way to account for these dynamics when predicting responses for the full assembly is to use an experimental subcomponent model. However, few methods have been proposed to identify and utilize nonlinear subcomponent models in substructuring.

In Part I the authors outlined a method used for testing and identifying weakly nonlinear structures that can be modeled as a collection of uncoupled, weakly nonlinear (in the case of micro-slip) oscillators. This work builds on that using the identified nonlinear modal models to describe subcomponents in an experimental-analytical dynamic substructuring prediction. A more in depth study of these modal models is contained in [1]. Experimental identification of nonlinear modal models has also been explored previously on an industrial system in [2] using 4-parameter modal Iwan models. More, recently the Iwan modal models have been compared with polynomial models in [3, 4].

Sandia National Laboratories is a multi-program laboratory managed and operated by Sandia Corporation, a wholly owned subsidiary of Lockheed Martin Corporation, for the U.S. Department of Energy's National Nuclear Security Administration under contract DE-AC04-94AL85000.

D. Roettgen (✉) • M.S. Allen • D. Kammer
Department of Engineering Physics, University of Wisconsin, Madison, WI 53706, USA
e-mail: droettgen@wisc.edu; msallen@engr.wisc.edu; kammer@engr.wisc.edu

R.L. Mayes
Structural Dynamics Department, Sandia National Laboratories, P.O. Box 5800 – MS0557, Albuquerque, NM 87185, USA
e-mail: rlmayes@sandia.gov

M.S. Allen et al. (eds.), *Dynamics of Coupled Structures, Volume 4*, Conference Proceedings of the Society for Experimental Mechanics Series, DOI 10.1007/978-3-319-54930-9_16

There are several methods of experimental-analytical substructuring. In [5] deKlerk and Rixen discuss many methods and their history. The synthesis procedures in these techniques apply to both linear and nonlinear systems. In the work described herein, the transmission simulator method was used to generate dynamic substructuring predictions. This method uses an experimental system that includes a fixture (or transmission simulator) as one subcomponent. This fixture is meant to simulate the boundary conditions of the subcomponent of interest in the next level assembly. The rationale behind the transmission simulator method can be found in [6–8]. One main advantage of this method is its ability to capture the stiffness and damping between the substructures because the same joint is used between the transmission simulator and the structure of interest as that in the full assembly. Here this is especially important because it allows one to capture the nonlinearity generated by the joint in a single experimental substructure, using the transmission simulator to excite the joint dynamics. This means that one can capture the nonlinearities in the system on the subcomponent level, then assemble the substructure models to see how those nonlinear forces affect the fully assembled structure.

A few methods have been explored for completing synthesis with nonlinear components. In [9] Kalaycioglu and Ozguven discuss component mode synthesis with nonlinear structural modifications. More recently, Krack explored using component mode synthesis with nonlinear normal modes in [10]. This work focuses on weakly nonlinear structures where the modes remain uncoupled in microslip amplitude ranges. This is the first attempt to use these nonlinear modal models in a synthesis approach using the transmission simulator method and weakly nonlinear modes. This is a continuation based on the approach presented by the authors in [11].

Substructuring methods are not yet commonly used in industry, but in most applications practitioners seek to create finite element models of the structure of interest, possibly including nonlinearities, and to update the model to reproduce the available experimental measurements. This alternative is also briefly explored here by modeling the Brake-Reuss Beam with a discrete Iwan joint to represent the area around each bolt. The parameters of these models are then updated to best match test data. This also provides a model that can be used to simulate modal substructuring on the Brake-Reuss Beam. In a companion paper [12] this same approach is used to predict the response of the Brake-Reuss Beam after modifying part of the structure away from the joint.

This paper is organized as follows. Sect. 16.2 outlines the theory behind dynamic substructuring when using these nonlinear modal models. Sect. 16.3 contains an overview of the substructuring problem being investigated as well as detailed descriptions of each substructure. In Sect. 16.4 these substructuring techniques are employed on both a FEM assembly and experimental-analytical assembly of the Brake-Reuss Beam. Section 16.5 concludes the paper and discusses some future work in this research area.

16.2 Nonlinear Modal Substructuring Using the Transmission Simulator Method

This section begins with a discussion on traditional linear dynamic substructuring, then the nonlinear forces are implemented into the problem as described later. Traditional substructuring is explained well in [13] and [5], but an overview is provided here for convenience. For a general linear system, each substructure can be written as

$$\mathbf{M}_C\ddot{\mathbf{x}}_C + \mathbf{C}_C\dot{\mathbf{x}}_C + \mathbf{K}_C\mathbf{x}_C = \mathbf{F}_C \tag{16.1}$$

where, $\mathbf{M}_C$, $\mathbf{C}_C$, and $\mathbf{K}_C$ are the mass, damping and stiffness matrices of substructure C. This work implements modal substructuring so this equation of motion is now cast into modal space by using the modal transformation where the physical displacements, $\mathbf{x}_C$, on substructure C are related to the mode shapes and modal coordinates, $\mathbf{q}_C$, of the substructure. This transformation is completed by using the linear mode shape matrix, $\boldsymbol{\phi}_C$.

$$\mathbf{x}_C = \boldsymbol{\phi}_C\mathbf{q}_C \tag{16.2}$$

After making this substitution and premultiplying by the transposed mode shape matrix the equations of motion for the substructure leads to the modal equations of motion presented in Eq. (16.3).

$$\mathbf{I}_C\ddot{\mathbf{q}}_C + \left[\backslash(2\zeta_C\omega_{n,C})\backslash\right]\dot{\mathbf{q}}_C + \left[\backslash\left(\omega_{n,C}^2\right)\backslash\right]\mathbf{q}_C = \boldsymbol{\phi}_C{}^T\mathbf{F}_C \tag{16.3}$$

The transmission simulator method begins by writing the modal equations of motion for each substructure in block diagonal form as shown in Eq. (16.4). Note that as shown, substructure C and B are positive and substructure A is negative

in the block diagonal; this is the common transmission simulator scenario where one is adding two substructures together and removing the effects of the transmission simulator from the system.

$$\begin{bmatrix} \mathbf{I}_C & 0 & 0 \\ 0 & \mathbf{I}_B & 0 \\ 0 & 0 & -\mathbf{I}_A \end{bmatrix} \begin{Bmatrix} \ddot{\mathbf{q}}_C \\ \ddot{\mathbf{q}}_B \\ \ddot{\mathbf{q}}_A \end{Bmatrix} + \begin{bmatrix} \backslash(2\zeta_C\omega_{n,C})_\backslash & 0 & 0 \\ 0 & \backslash(2\zeta_B\omega_{n,B})_\backslash & 0 \\ 0 & 0 & \backslash(-2\zeta_A\omega_{n,A})_\backslash \end{bmatrix} \begin{Bmatrix} \dot{\mathbf{q}}_C \\ \dot{\mathbf{q}}_B \\ \dot{\mathbf{q}}_A \end{Bmatrix} + \begin{bmatrix} \backslash(\omega_{n,C}^2)_\backslash & 0 & 0 \\ 0 & \backslash(\omega_{n,B}^2)_\backslash & 0 \\ 0 & 0 & \backslash(-\omega_{n,A}^2)_\backslash \end{bmatrix} \begin{Bmatrix} \mathbf{q}_C \\ \mathbf{q}_B \\ \mathbf{q}_A \end{Bmatrix} = \begin{Bmatrix} \boldsymbol{\phi}_C{}^T\mathbf{F}_C \\ \boldsymbol{\phi}_B{}^T\mathbf{F}_B \\ \boldsymbol{\phi}_A{}^T\mathbf{F}_A \end{Bmatrix} \tag{16.4}$$

Note that each substructure in the equations above is uncoupled from the other components. Additionally, each mode of each substructure is uncoupled from the other modes. In order to complete dynamic substructuring we must enforce constraints between the individual substructures which can be written as follows.

$$\mathbf{B} \begin{bmatrix} \mathbf{x}_C \\ \mathbf{x}_B \\ \mathbf{x}_A \end{bmatrix} = 0 \tag{16.5}$$

These constraints tie physical degrees of freedom on different substructures to enforce displacement compatibility at the interface between substructures. Here, $\mathbf{B}$, is a Boolean matrix that defines this compatibility. These constraints can be cast into the modal domain as shown in Eq. (16.6).

$$\mathbf{B} \begin{bmatrix} \boldsymbol{\phi}_\mathrm{C} & 0 & 0 \\ 0 & \boldsymbol{\phi}_\mathrm{B} & 0 \\ 0 & 0 & \boldsymbol{\phi}_A \end{bmatrix} \begin{bmatrix} \mathbf{q}_C \\ \mathbf{q}_B \\ \mathbf{q}_A \end{bmatrix} = 0 \tag{16.6}$$

Then a new set of coordinates, $\boldsymbol{\eta}$, are defined that can take on any values without violating the constraints. This is accomplished by finding a transformation matrix, $\mathbf{L}$, that resides in the nullspace of $\overline{\mathbf{B}}$.

$$\mathbf{q} = \mathbf{L}\boldsymbol{\eta} \tag{16.7}$$

$$\mathbf{B} \begin{bmatrix} \boldsymbol{\phi}_\mathrm{C} & 0 & 0 \\ 0 & \boldsymbol{\phi}_\mathrm{B} & 0 \\ 0 & 0 & \boldsymbol{\phi}_A \end{bmatrix} \mathbf{L} \begin{bmatrix} \boldsymbol{\eta}_C \\ \boldsymbol{\eta}_B \\ \boldsymbol{\eta}_A \end{bmatrix} = \overline{\mathbf{B}}\mathbf{L} \begin{bmatrix} \boldsymbol{\eta}_C \\ \boldsymbol{\eta}_B \\ \boldsymbol{\eta}_A \end{bmatrix} = 0 \tag{16.8}$$

$$\mathbf{L} = null\left(\overline{\mathbf{B}}\right) \tag{16.9}$$

This transformation matrix can now be applied to the modal equations of motion, Eq. (16.4), to synthesize the system.

$$\overline{\mathbf{M}}\ddot{\boldsymbol{\eta}} + \overline{\mathbf{C}}\dot{\boldsymbol{\eta}} + \overline{\mathbf{K}}\boldsymbol{\eta} = \mathbf{L}^T \begin{Bmatrix} \boldsymbol{\phi}_C{}^T\mathbf{F}_C \\ \boldsymbol{\phi}_B{}^T\mathbf{F}_B \\ \boldsymbol{\phi}_A{}^T\mathbf{F}_A \end{Bmatrix} \tag{16.10}$$

In Part I, the authors explored representing a single substructure as a combination of linear and weakly nonlinear modes. Thus the equations of motion for such a substructure could be written as:

$$\begin{aligned} \mathbf{I}_C\ddot{\mathbf{q}}_C + \left[\backslash(2\zeta_C\omega_{n,C})_\backslash\right]\dot{\mathbf{q}}_C + \left[\backslash(\omega_{n,C}^2)_\backslash\right]\mathbf{q}_C + \{\mathbf{F}_{NL,C}\} &= \boldsymbol{\phi}_C{}^T\mathbf{F}_C \\ \{\mathbf{F}_{NL,C}\}^\mathrm{T} &= [F_{NL,1,C}\,(q_{1,C}) \quad F_{NL,2,C}\,(q_{2,C}) \quad \cdots]^\mathrm{T} \end{aligned} \tag{16.11}$$

where, $F_{NL,n,C}(q_{n,C})$, is an force describing the joint nonlinearity of the n$^{\text{th}}$ mode based on the state of that modes amplitude. This could take many forms but in this work this force is represented by a 4-parameter modal Iwan model. Each mode of the subcomponent is still treated as uncoupled; thus the authors assume the mode shapes do not change with increased force level

and that the modes of the system remain uncoupled. This limits this methodology to substructuring with weakly nonlinear substructures. As first proposed in [11], these joint forcing terms can be added to the synthesized equations through the same transformation matrix.

$$\overline{\mathbf{M}}\ddot{\boldsymbol{\eta}} + \overline{\mathbf{C}}\dot{\boldsymbol{\eta}} + \overline{\mathbf{K}}\boldsymbol{\eta} + \mathbf{L}^T \begin{Bmatrix} \mathbf{F}_{NL,C} \\ \mathbf{F}_{NL,B} \\ \mathbf{F}_{NL,A} \end{Bmatrix} = \mathbf{L}^T \begin{Bmatrix} \boldsymbol{\phi}_C{}^T \mathbf{F}_C \\ \boldsymbol{\phi}_B{}^T \mathbf{F}_B \\ \boldsymbol{\phi}_A{}^T \mathbf{F}_A \end{Bmatrix} \tag{16.12}$$

Also note that the nonlinear forces themselves depend on the substructure DOF $\mathbf{q}_C$, $\mathbf{q}_B$ and$\mathbf{q}_A$, which are related to $\boldsymbol{\eta}$ via eq. (16.7). In Part I [1], each modal DOF remained uncoupled and hence the response of the substructure could be found by integrating each SDOF modal equation of motion independent of the others. However, when assembling the substructures these nonlinear forces are spread to all DOF via $\mathbf{L}^T$ and thus the modal DOF are no longer uncoupled in the assembled system. In [11] the authors detail specifically how to implement these with the use of a 4-parameter Iwan modal model in a Newmark integration algorithm, so that is not repeated here. In the next section, the authors define each substructure studied in this work, the Brake-Reuss Beam.

16.3 Substructure Identification

With dynamic substructuring theory in place, this section will discuss the individual substructures of interest for this study. The system of interest for this study is the Brake-Reuss Beam which is a pair of metallic half-beams bolted at the center with a lap joint. Figure 16.1 shows the Brake-Reuss Beam in an experimental set-up.

Figure 16.2 shows the three substructures and the built-up, modified structure. Substructure C is the standard Brake-Reuss Beam that is represented by: (1) an experimental model, detailed in [1], (2) a FEM model discussed in Sect. 16.3.2 of this work. Substructure A will be the transmission simulator for these predictions and is simply the right half of the Brake-Reuss Beam system. This substructure is modeled using a finite element model, detailed in Sect. 16.3.3. Substructure B is a design modification, a half beam with a mass attached to the end. Finally, the assembly of interest is the modified Brake-Reuss Beam represented by substructure D.

The goal is to predict the dynamics of a modified Brake-Reuss Beam (substructure D) in which the right beam (substructure A) is replaced with a modified structure (substructure B). This simulates an industrial application where a design modification is made to one part of the assembly such that its dynamics are changed considerably. This task was completed following two parallel paths where substructure C is embodied using two different methods. The first path

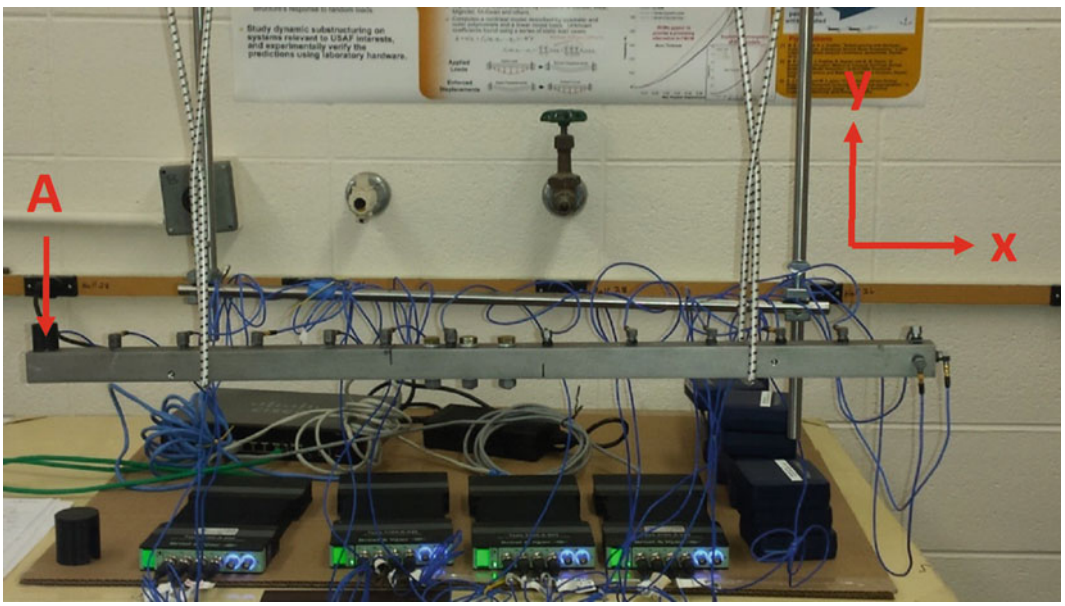

Fig. 16.1 Brake-Reuss Beam experimental set-up

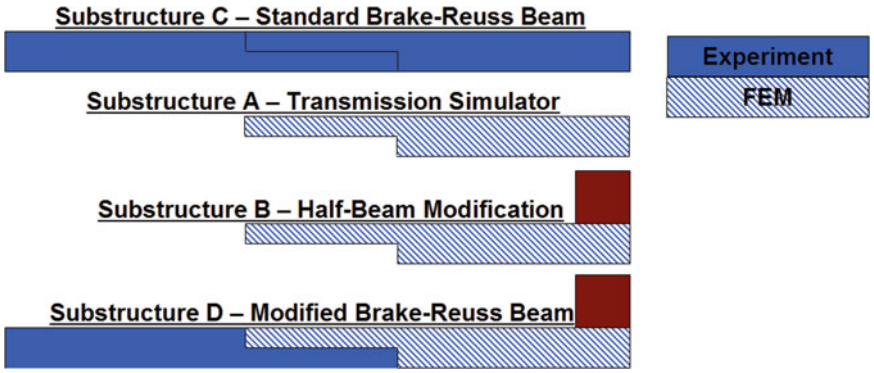

Fig. 16.2 Substructure overview

Table 16.1 Substructure designation

	FEM substructuring	Experimental-analytical substructuring
Substructure C:Standard BRB	FEM	Experiment
Substructure A:Transmission Simulator	FEM	FEM
Substructure B:Half-Beam Modification	FEM	FEM
Substructure D: Comparison for Prediction	Full Simulation	Truth Test

Table 16.2 System C experimental parameters [1]

Modal index	Natural frequency [Hz]	Damping ratio	Linear or nonlinear	F_s	K_T	β	χ
1	172.70	0.00095	Nonlinear	137.7	484,680	0.2616	−0.04995
2	583.26	0.00143	Nonlinear	152.1	2,668,200	0.2969	−0.4164
3	1180.10	0.00376	Linear	–	–	–	–
4	1645.40	0.00814	Linear	–	–	–	–

utilized a FEM of the substructure where three discrete nonlinear Iwan joints were included between the two substructures to represent the bolts. The four parameters describing each Iwan joint were updated to match experimental response measurements. The second is a combined experimental-analytical substructure where the nonlinear modal model from Part I [1] is employed. Both paths will attempt to utilize their respective substructure models in order to predict the response of a modified Brake-Reuss Beam, substructure D.

Table 16.1 shows the source of each substructure for the two substructuring paths. When completing substructuring with the FEM model, the response prediction will be compared to a response generated from a full FEM simulation. For the experimental-analytical substructuring, the predicted response will be compared to the measured response from a truth test. The following subsections will provide the identification for each substructure used in these predictions.

16.3.1 Experimental Substructure C: Standard Brake-Reuss Beam

Substructure C is the standard Brake-Reuss Beam which was studied in detail in Part I [1], but a brief summary is contained here. The Brake-Reuss Beam was instrumented with 15 low sensitivity (5 mV/g) accelerometers as shown in Fig. 16.1. A low level modal test was used in order to determine the linear parameters of the system as listed in Table 16.2. High level impact testing was used to fit nonlinear modal models for the first and second elastic modes of the substructure. As detailed in Part I, only the first two elastic modes of the system were found to behave nonlinearly and thus were modeled with 4-parameter Iwan modal models (i.e. an Iwan joint in parallel with the modal stiffness and damping, as shown in Fig. 16.3). The experimentally extracted Iwan parameters are repeated Table 16.2 for convenience.

Each mode of the system is uncoupled from all others, so each can be represented as a single degree of freedom oscillator as shown in Fig. 16.3. *Fj* is an instantaneous force in the Iwan Joint which can be found as described by Segalman in [14].

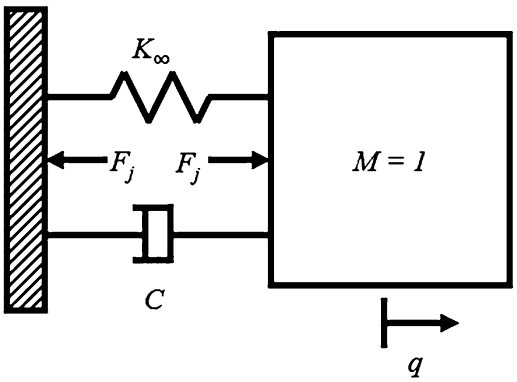

Fig. 16.3 Schematic of SDOF model used for each modal degree of freedom

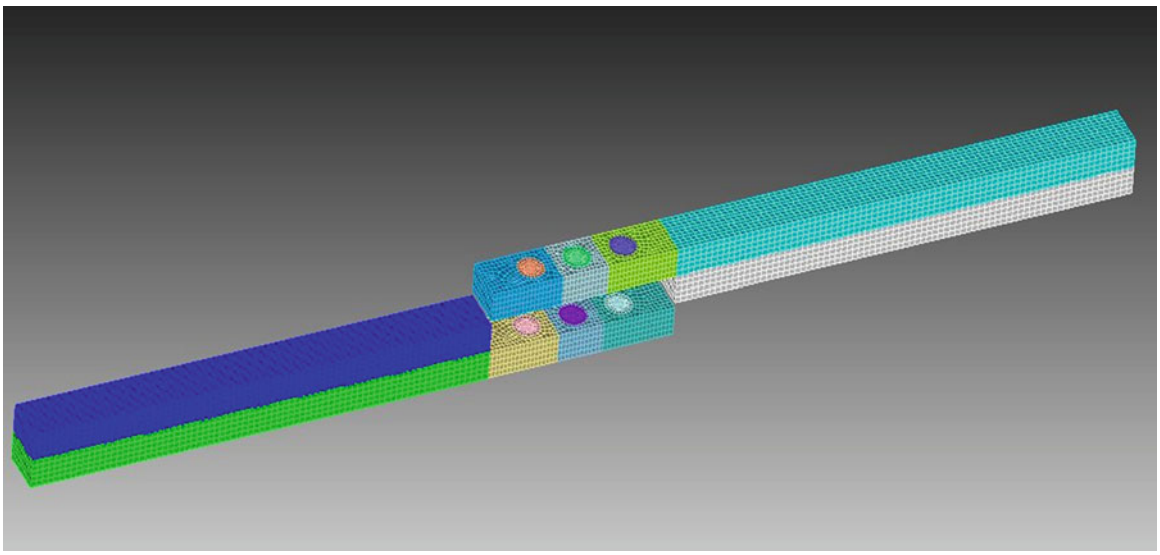

Fig. 16.4 Finite element mesh for Brake-Reuss Beam substructure C

These Iwan parameters were obtained by fitting amplitude dependent stiffness and damping curves from several high level impact tests. The same high level testing data was used to calibrate the next substructure, the numerical FEM model of substructure C.

16.3.2 Numerical Substructure C: Standard Brake-Reuss Beam

A finite element model of substructure C was also developed. This allowed the authors to determine how accurate modal substructuring could be when experimental error is removed from the predictions. A solid mesh was made of the Brake-Reuss Beam system using 22,000 elements, as shown in Fig. 16.4. The half beams of the system were modeled and meshed separately at this stage.

In order to connect the two half beams, the joint surfaces were connected to a virtual node using averaging rigid bar elements (i.e. RBE3 in Nastran). These spider-like connections are shown in Fig. 16.5. At these virtual nodes, a set of linear springs and an Iwan joint in the axial direction was added to the system in order to couple the two beams.

A Craig-Bampton (CB) model was extracted from the FEM program. This model was derived from the model used by Gross, Lacayo, et al. in [15]. The CB model contained 30 fixed interface modes and the three virtual nodes at interface locations with 6 degrees of freedom each. After the CB model was extracted, linear springs were added between the two beams except in the axial direction. At each of the three virtual nodes, the DOFs in the axial direction were instead coupled using a 4-parameter Iwan model. The parameters of these discrete Iwan elements will later be updated to match experimental measurements from the assembled Brake-Reuss Beam. Note that, although one could connect each pair of the nodes at the joint surface with a nonlinear element, this would be contrary to the idea of using an Iwan element, which internally contains a parallel array of slider elements that are tuned to represent the stiffness and damping of an entire joint.

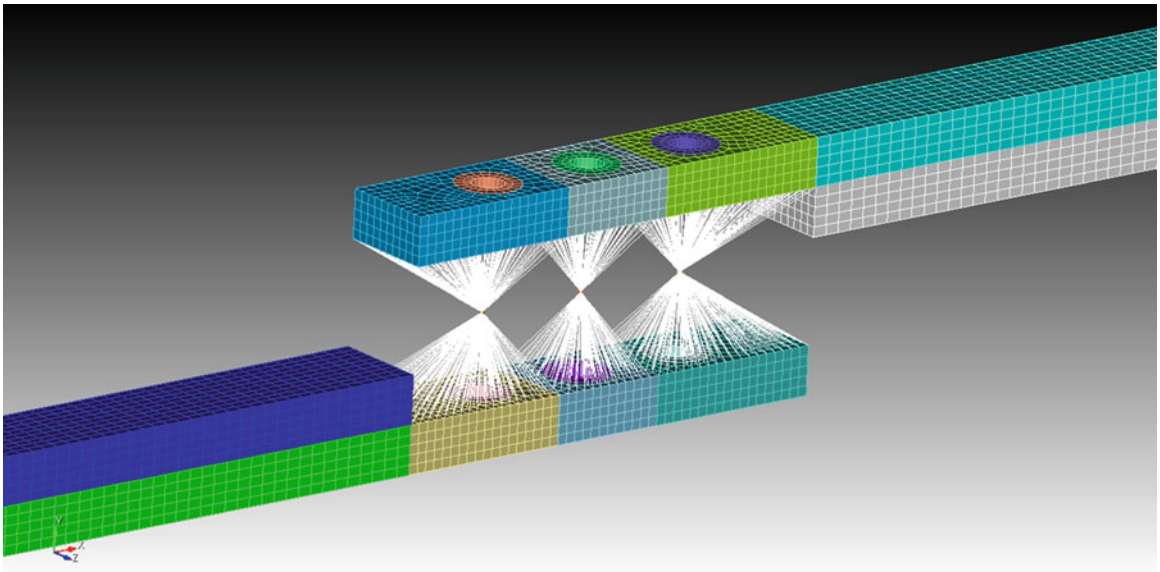

Fig. 16.5 Finite element joint surface spider-patch

Table 16.3 System C experimental parameters

Modal index	Experimental natural frequency [Hz]	FEM natural frequency [Hz]	Frequency % Error	MAC
1	172.70	172.09	−0.35%	0.9994
2	583.26	578.53	−0.81%	0.9975
3	1180.10	1195.20	1.28%	0.9962
4	1645.40	1616.10	−1.78%	0.9897

The two beams were assembled as described above with the Iwan elements represented by springs with the low amplitude stiffness, $\mathbf{K}_0$, and the eigen value problem was solved to obtain the natural frequencies and mode shapes, see Table 16.3. Also included in Table 16.3 are the MAC values between the FEM and experimental mode shapes. The model matches very well with frequency errors under 2% and MAC values above .98 for all the modes of interest. Figure 16.6 shows a comparison for the first two elastic modes between the FEM model and the experimentally extracted mode shapes.

In [16] Allen, Lacayo and Brake presented an adaptation of the quasi-static algorithm of [17] that statically loads a structure in the shape of a mode to excite one mode of interest. The study in [16] showed that this algorithm accurately estimates the behavior of each mode of a typical structure in a small fraction of the time required to perform a dynamic simulation. The authors made use of this algorithm to calibrate the parameters of the three discrete Iwan joints of the assembled Craig-Bampton model by matching the amplitude dependent natural frequency and damping curves for the first two elastic modes extracted from the FEM with the corresponding curves extracted from the measured impact data as outlined in Part I [1]. Figure 16.7 shows the results of this quasi-static simulation for the first elastic mode of substructure C.

After manual trial and error, the Iwan parameters for the three discrete joints were found and are given in Table 16.4.

In order to simulate experimental modal substructuring for this model, simulated experimental measurements were needed from which a SDOF nonlinear model could be estimated for each mode. For convenience, the quasi-static solutions (such as that shown in Fig. 16.7 for Mode 1) were fit to a 4-parameter modal Iwan model for each mode. Recall that in Part I [1], only the first two elastic modes in the experimental system were observed to exhibit measurable nonlinearity. However, when a structure contains even one nonlinear element, all bending modes can end up exhibiting some traces of nonlinearity. Such was the case here, so a nonlinear modal model was fit to each of the four bending modes. Table 16.5 contains the parameters for the four elastic modes of the numerical version of substructure C. These four nonlinear elastic modes in combination with 2 rigid modes comprise the numerical model of the system.

It is interesting to consider why the experimental model did not show similar evidence of nonlinearity in the 3rd and 4th bending modes. One possible explanation is that perhaps the force level applied during the experiments was not adequate to excite the nonlinearity in the 3rd and 4th bending modes. Conversely, it could be that the discrete Iwan elements used here are not a perfect model for the actual beam. This numerical substructure is only used to prove out nonlinear substructuring techniques. As such, it was necessary to tune the Iwan parameters to get realistic amplitude dependant results, but not perfectly match the experimental results.

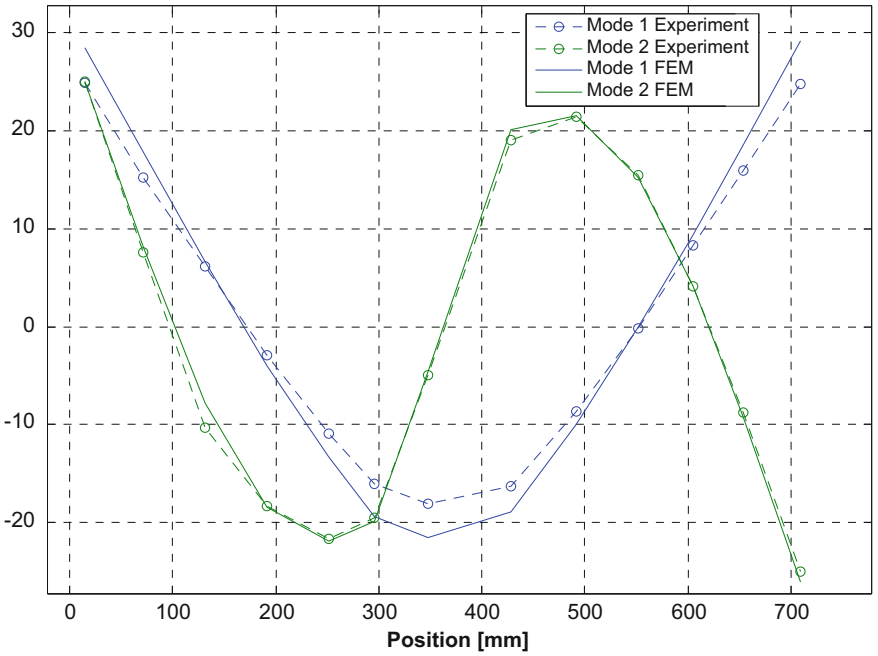

Fig. 16.6 FEM and experimental mode shapes

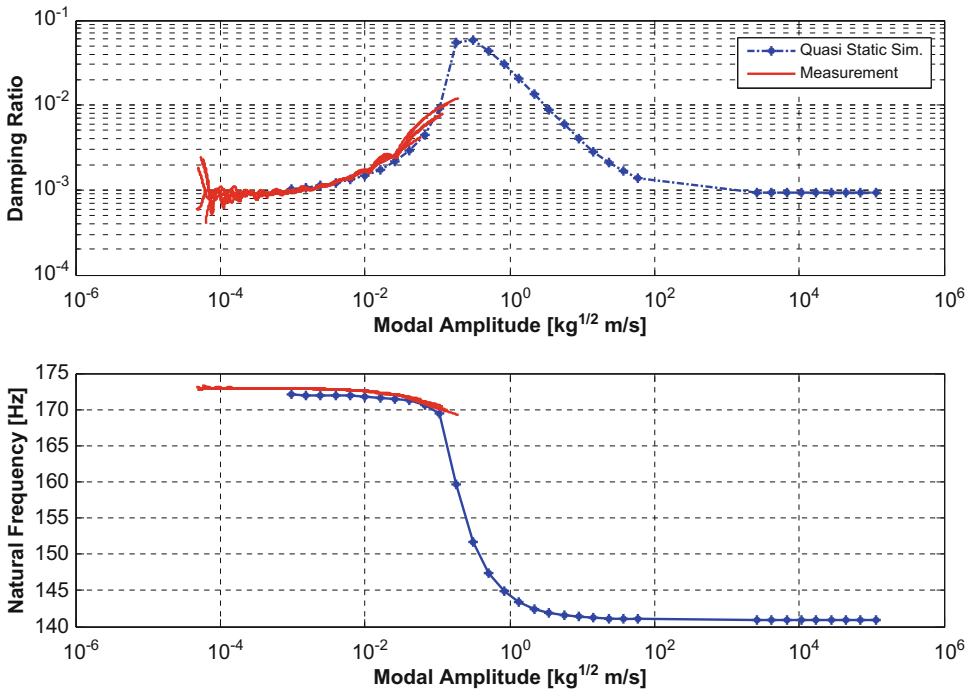

Fig. 16.7 Quasi-Static results for amplitude dependent damping and frequency

Table 16.4 System C Discrete Iwan parameters

Joint #	F_s	K_T	β	χ
1	25	2,200,000	–.3500	0.0500
2	10	1,840,000	–.9000	0.0500
3	25	2,200,000	–.3500	0.0500

Table 16.5 Substructure C numerical FEM parameters

Modal index	Natural frequency [Hz]	Damping ratio	Linear or nonlinear	F_s	K_T	β	χ
1	171.26	0.0010	Nonlinear	30.50	385,920	4.25	–0.13546
2	578.28	0.0010	Nonlinear	250.01	927,330	1.25	–0.72461
3	1195.20	0.0010	Nonlinear	3297.4	9,322,300	0.25	–0.25792
4	1616.10	0.0010	Nonlinear	39,000	77,249,000	0.25	–0.69576

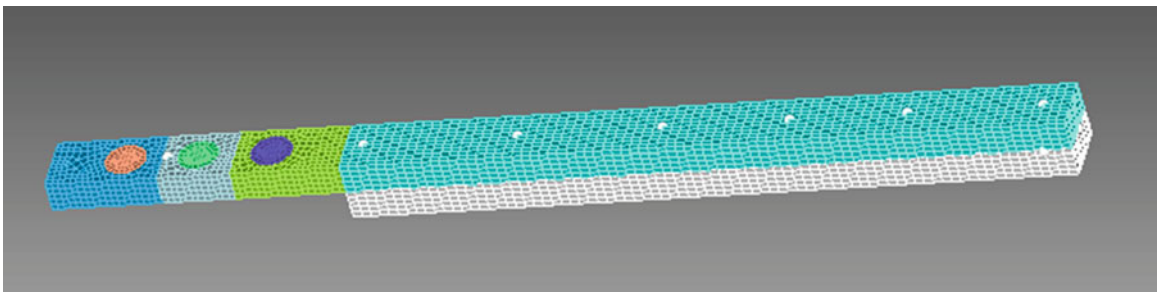

Fig. 16.8 FEM and experimental mode shapes

Table 16.6 Modified system frequency shifts

Modal index	Substructure A [Hz]	Substructure B [Hz]	% Change	Substructure C (Linear FEM) [Hz]	Substructure D (Linear FEM) [Hz]	% Change
1	623.37	539.12	–13.52%	171.26	151.83	–11.35%
2	1438.72	1134.38	–21.15%	578.28	578.28	–10.85%
3	3033.48	2295.71	–24.32%	1195.20	1195.20	–15.71%
4	4562.07	3930.13	–13.85%	1616.10	1616.10	–6.04%

16.3.3 Substructure A and B: Standard and Half-Beam Modification

The transmission simulator and half-beam modification were modeled in a finite element program. The first is a simple half-beam from the Brake-Reuss Beam system. This substructure will act as the transmission simulator, so modal constraints will be used to couple the negative copy of this substructure to the measured transmission simulator at all measurement points. Thus its effects will be removed from the assembly during the substructuring process. Figure 16.8 shows the finite element mesh for the transmission simulator. The nodes shown in white depicted on Fig. 16.8 the are the measurement points.

Recall from Fig. 16.2 that the transmission simulator will be replaced with the half-beam modification in the assembly of interest. In order to verify that substructures A and B are sufficiently different so that the substructuring problem is not trivial, their natural frequencies were compared and the results are shown in Table 16.6. Each natural frequency shifts by at least 13% (more than 100 times the width of the peak in the FRF), so the change is judged to be adequate to provide an interesting case study. A 0.75 kg mass was attached to the end of the beam to sufficiently shift the frequencies of the first few bending modes of the system. Material damping of 0.1% was used for each mode in the standard and modified transmission simulator.

Figure 16.9 displays the FEM mesh of the half-beam modification. The added mass was connected to the beam using high stiffness springs between each pair of adjoining nodes.

16.4 Nonlinear Modal Substructuring Results

Next, the transmission simulator equations, Eqs. (16.11) and (16.12) were used to generate predictions of the modified assembly (substructure D). First, predictions were constructed using the numerical model and compared to the full FEM simulation, as detailed in Sect. 16.4.1. With the numerical model it is simple to test different scenarios such as sensor placement and the number of modes retained in each substructure. This also gives an indication of how well this method can work in the absence of experimental noise. The process was repeated using the experimental-analytical substructuring approach in Sect.16.4.2. These experimental-analytical predictions are compared directly to measured test data to assess their quality.

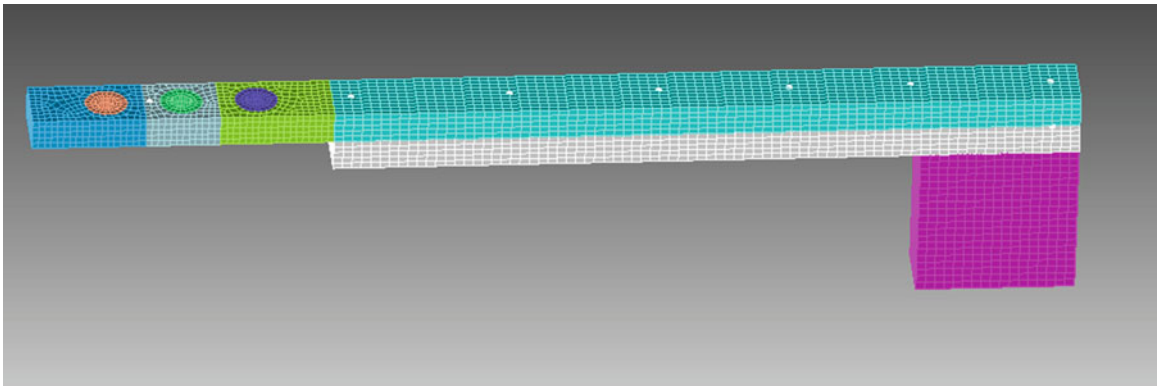

Fig. 16.9 FEM and experimental mode shapes

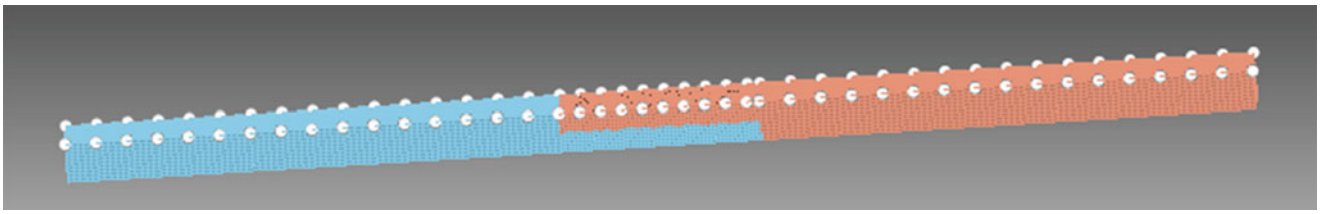

Fig. 16.10 FEM with expanded sensor selection

Table 16.7 Numerical linear substructuring predictions

Elastic mode #	Full FEM frequency [Hz]	Substr. prediction frequency [Hz]	% Error
1	151.83	148.57	–2.39%
2	515.55	515.37	–1.00%
3	1007.37	1037.12	1.72%
4	1518.52	1519.61	0.72%

16.4.1 Numerical Substructuring Results

With the numerical model of Substructure C, it was possible to use as many nodes as desired in the simulation. The authors selected a reduced set to best simulate an experiment where finite instrumentation pieces may limit sensor locations. In order to evaluate modal convergence for each substructure, this large sensor set was used. This provides high quality mode shapes even for higher order bending modes. Figure 16.10 shows an expanded set of degrees of freedom used in the numerical substructuring.

A study was completed to determine how many modes of each substructure were needed for a high-quality, linear prediction. Table 16.7 shows the linear frequencies that this substructuring model predicts for the first four elastic modes. For this case, 6 modes (2 rigid and 4 elastic) were used in each of substructures C and B; while only 4 modes (2 rigid and 2 elastic) were used for the transmission simulator. The frequencies are reasonably accurate, suggesting that modal truncation will not be too severe if at least four elastic modes can be measured.

The number of modes in each substructure was varied to understand how sensitive the results were to the particular modes used for each substructure. Table 16.8 shows several of the combinations evaluated. Here, Case #1 is case that was just discussed. A few important observations may be made. Cases #4 and #7 show that the error increases significantly if the 4th mode of A it not included. Cases #9-#11 can be compared to Case #3 and we can see that additional modes in substructure C do not improve the quality of the prediction. The configuration from Case #3 was chosen to evaluate the nonlinear substructuring. This includes 6 modes in substructure C and B, but only 4 modes in the transmission simulator, substructure A.

Now that the number of modes to be retained in each substructure have been determined, the nonlinear forces can be added to the assembled equations of motion and a Newmark integrator can be used to predict the nonlinear response to 20 N impulsive loading at the center of the modified assembly (substructure D). The response was then decomposed into the contribution of each mode using a linear modal filter. A truth FEM was constructed using the same CB model of Substructure

Table 16.8 Mode convergence study

Case	# Modes in C	# Modes in A	# Modes in B	RMS Frequency % Error
1	6	6	6	0.911%
2	6	5	6	0.930%
3	6	4	6	0.798%
4	6	3	6	5.261%
5	6	5	5	0.813%
6	6	4	4	0.749%
7	6	3	3	4.682%
8	6	2	2	5.702%
9	7	4	6	0.798%
10	8	4	6	0.798%
11	9	4	6	0.797%

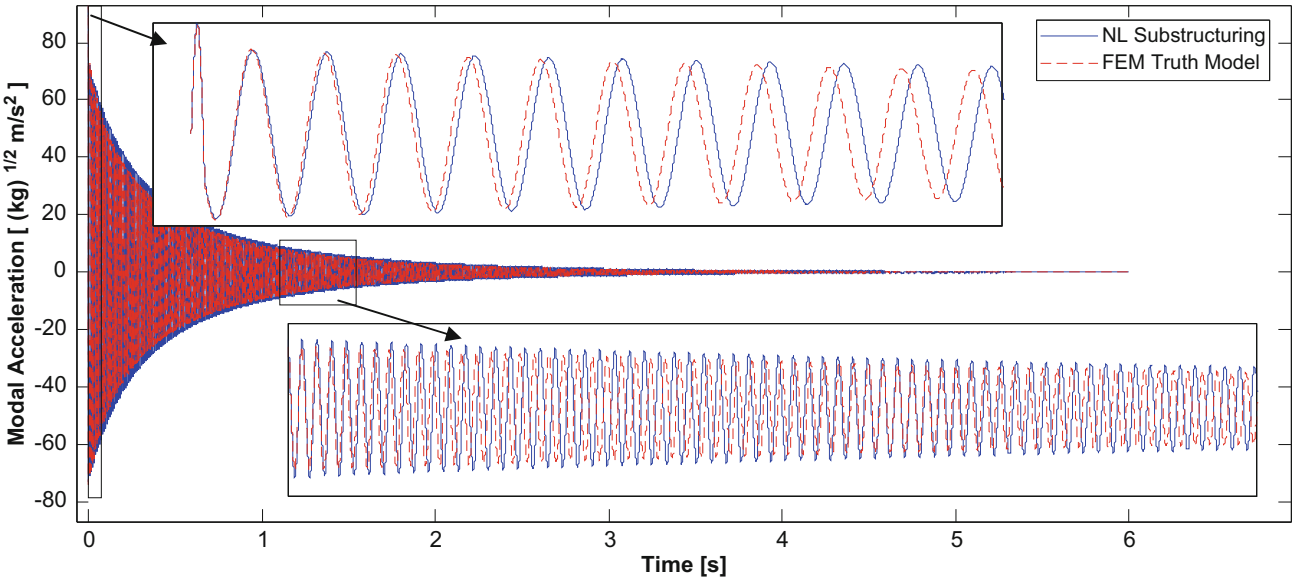

Fig. 16.11 1st Elastic mode: modal acceleration time history (Numerical Substructuring)

C with the transmission simulator, A, replaced with the half-beam modification, B. Note that the parameters of the three discrete Iwan joints were not altered when A was replaced with B as the discrete joint properties were believed to be unaffected by the modifications seen in B. The time histories for the first and second elastic modes are shown in Figs. 16.11 and 16.12. Both modes match the full truth FEM simulation remarkably well with the first elastic mode fitting slightly better than the second. The frequency for both modes is off slightly, but this is to be expected considering the frequency error present in Table 16.7.

These signals can be compared in the frequency domain as well by applying an FFT to the time history, as shown in Fig. 16.13. Here, the peaks between the nonlinear substructuring prediction and the full FEM solutions correlate well. A small nonlinear distortion is visible in both the substructuring prediction and the truth model and the only major source of error is due to a frequency shift in the linear substructuring prediction.

Additionally, the response predicted by substructuring can be compared to the full finite element simulation by way of the amplitude dependent natural frequency and damping ratio extracted from the time histories, as shown in Fig. 16.14. The frequency is normalized to the linear natural frequency to make the trends visually comparable despite the difference in the linear natural frequencies. Both the frequency and damping correlate well between the prediction and the FEM simulation for the 1st elastic mode.

The comparison was not so straightforward with the second mode. Figure 16.15 shows the amplitude dependent results for this mode. At higher amplitudes the curves have similar trends but at lower amplitudes the Hilbert algorithm apparently fails to accurately capture the frequency and damping. However, because the time signals and FFTs compared very well in Figs. 16.12 and 16.13 we suspect that this is simply an anomaly of the Hilbert algorithm.

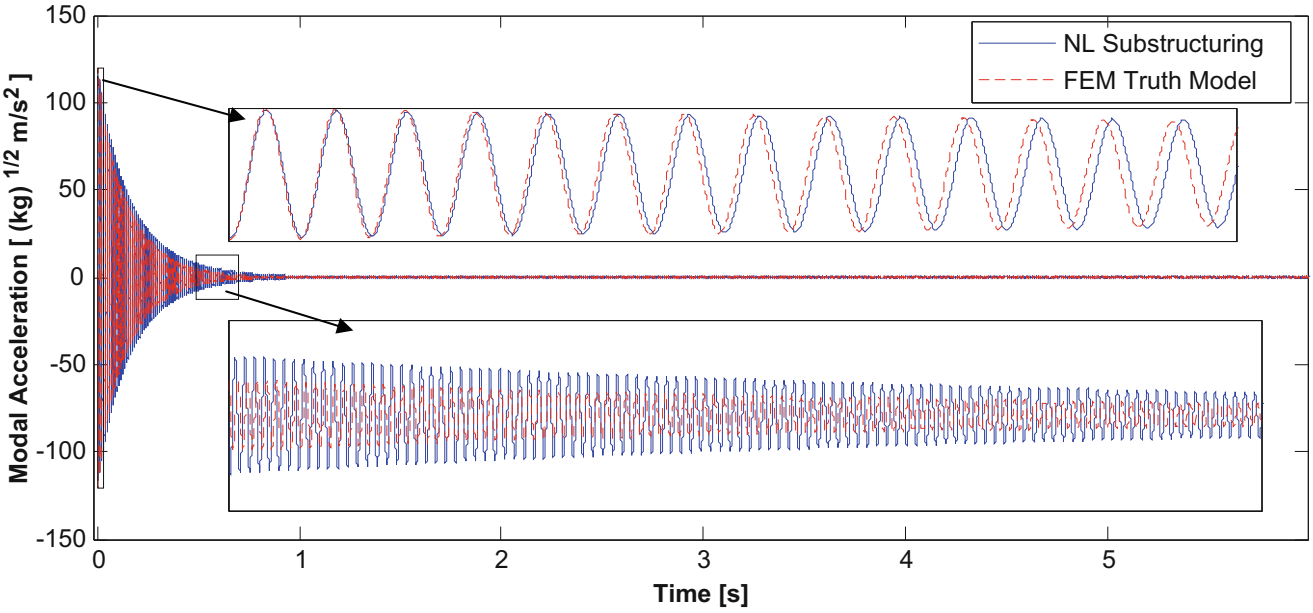

Fig. 16.12 2nd Elastic mode: modal acceleration time history (Numerical Substructuring)

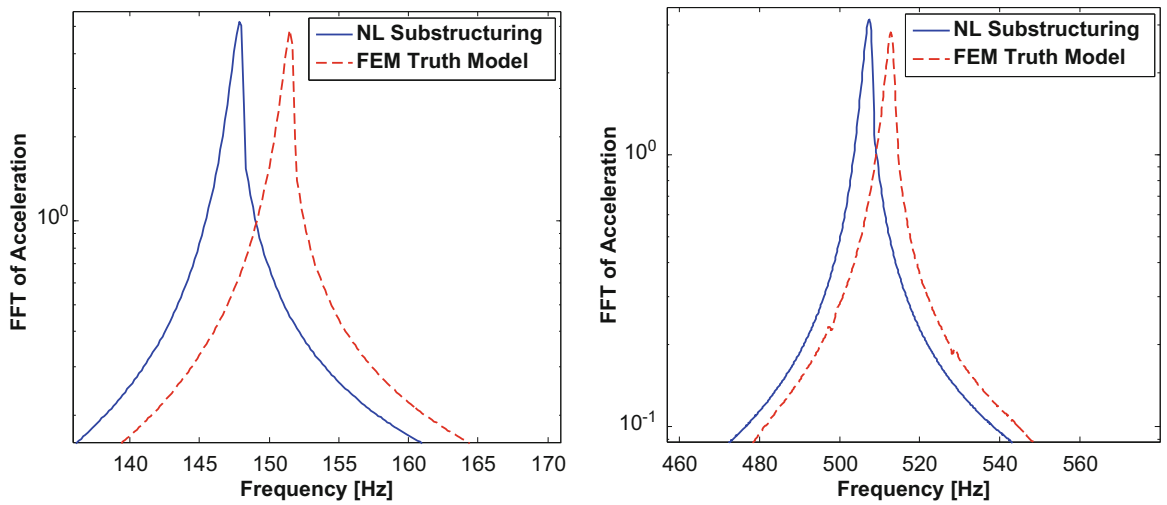

Fig. 16.13 FFT of modal acceleration for 1st (*right*) and 2nd (*left*) elastic modes

Overall, the nonlinear numerical substructuring prediction seemed to be a good estimate of the FEM solution. The simulation model suggests that nonlinear modal substructuring will work given an appropriate number of modes.

16.4.2 Experimental-Analytical Substructuring Results

To begin the experimental-analytical substructuring process the linear substructuring prediction is first completed. To do this the nonlinear forces for each mode were replaced with linear springs corresponding to the completely stuck state ($\mathbf{K}_0$). For this example, 6 modes each were retained for substructures C and B, with only 4 modes in substructure A. The predictions of the modal parameters of the first four elastic modes are compared with those from the truth test in Table 16.9. This captures how well a linear substructuring prediction did compared to a linear (low level) truth test!

In Table 16.9 the frequency errors are small. It is important to remember how much a mode changes due to the nonlinearity in the system. It is common to see frequency shifts around the 1–5% range due to high level impact testing. Thus, it may be

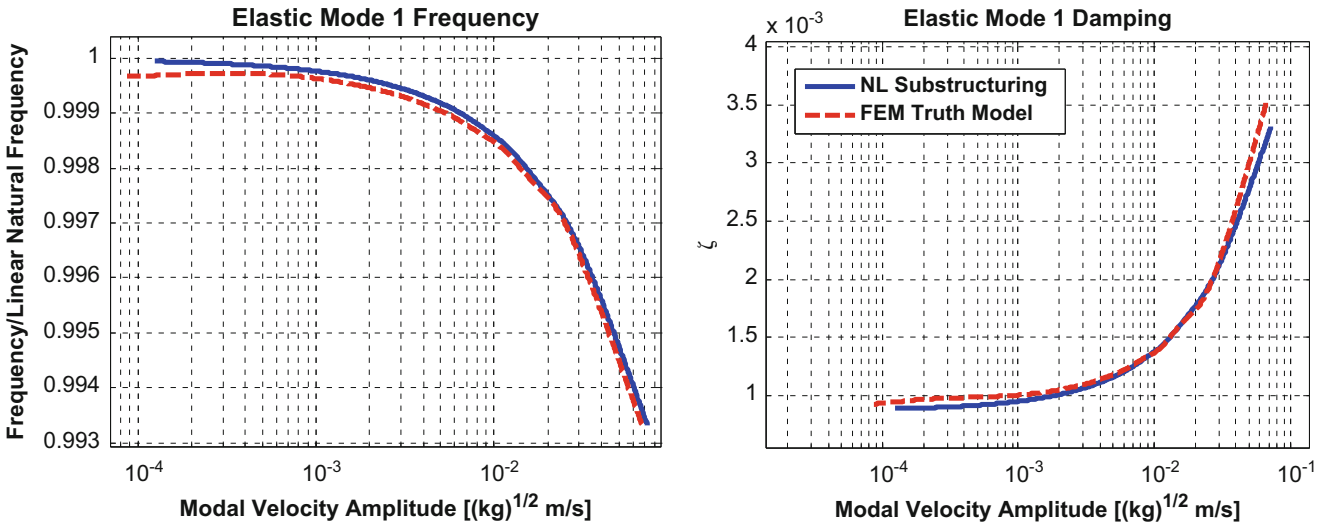

Fig. 16.14 Amplitude dependent frequency and damping - 1st elastic mode

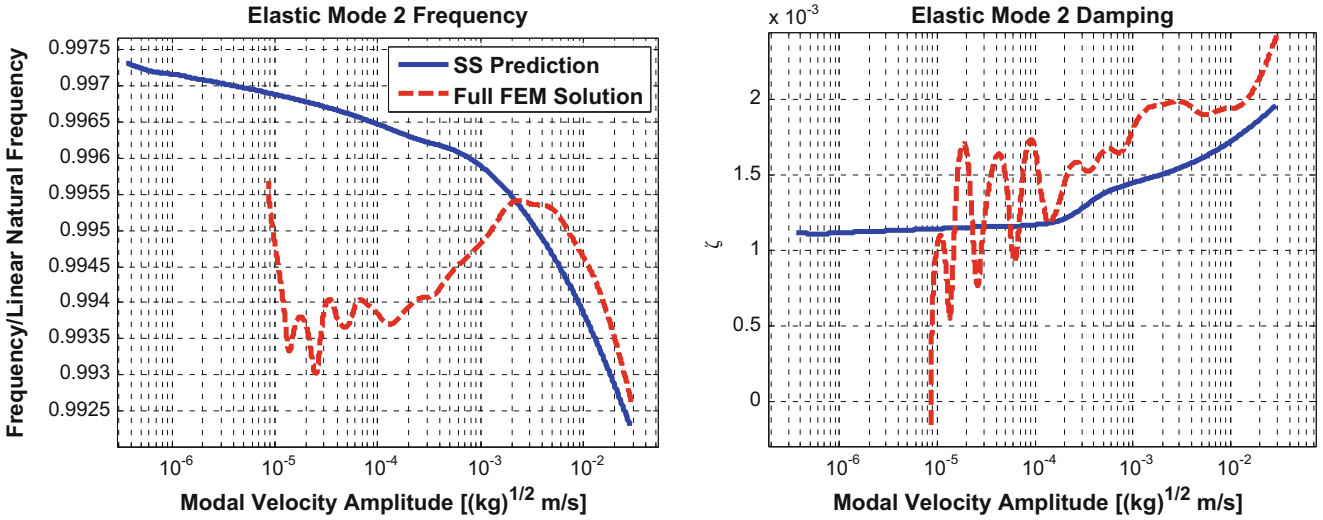

Fig. 16.15 Amplitude dependent frequency and damping - 2nd elastic mode

Table 16.9 Experimental-analytical linear substructuring predictions

Mode #	Linear truth test frequency [Hz]	Substr. prediction frequency [Hz]	% Error	Truth ζ	Substr. prediction ζ	% Error	MAC
1	150.80	153.13	1.54%	0.00194	0.00186	–3.98%	0.999
2	513.69	515.69	0.39%	0.00174	0.00141	–18.84%	0.991
3	994.68	983.23	–1.15%	0.00321	0.00339	5.72%	0.980
4	1507.53	1515.92	0.56%	0.00458	0.00668	45.99%	0.962

difficult to evaluate the effectiveness of the nonlinear modal models to capture the nonlinear stiffness. In contrast, damping errors in Table 16.9 are larger. Damping often changes by larger factors often being amplified by 200–400%. Although we have significant error in predicting damping, the error is small relative to how much the damping changes with amplitude. This change with amplitude is what we hope to represent with our nonlinear model.

The MAC values show that the modes correlate between the truth test and the substructured predictions very well. Figure 16.16 shows the modes shapes of the first two elastic modes. For each of these modes the prediction matches the experiment very well. Here, predicted modes are shown using the stuck ($\mathbf{K}_0$) case for the linear substructure and also the case when the

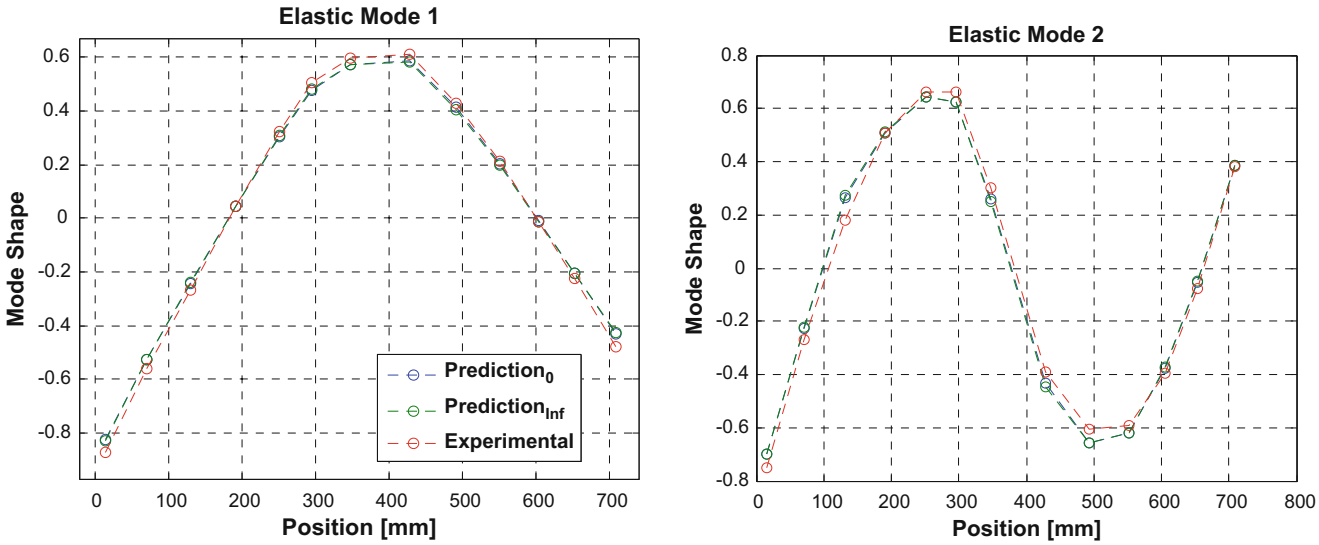

Fig. 16.16 Predicted mode shapes

joints are replace with springs corresponding to the fully slipped ($\mathbf{K}_\infty$) case. The mode shapes do not change in a measurable way between these two cases, revealing that the modes are apparently preserved at higher forcing levels even though the modal stiffness and damping have changed!

Now that the linear substructuring prediction quality is understood, the nonlinear forces can be added to the assembled equations of motion and a Newmark integrator can be used to predict the nonlinear response to 500 N impulsive loading at the end of the beam. Figure 16.17 compares the results of this response simulation in the frequency domain. The "Linear Measured" curve is a driving point FRF measurement for a low level test case, aiming to capture a linear driving point response. Another curve has been added to this plot which is the drive point frequency response function due to a 500 N impulsive load on the end of the beam. The difference between these two curves (green and red) are what the nonlinear modal models desire to replicate. The "Linear Substructuring Prediction" black curve is a curve fit of the modal parameters found from the linear substructuring process. Therefore, the shift between the green and black curves illustrates the error in the linear substructuring predictions.

When the nonlinear forces were added to the substructuring by using a Newmark integrator to solve Eq. (16.12) the impact of the nonlinear modal models became clear. The blue curve represents this nonlinear substructuring prediction. As mentioned previously, comparing the red and green curves highlights the change in the response due to the nonlinearity in the mode. Likewise comparing the blue and black curves highlights a similar change exists in the substructured predictions. The frequency of the nonlinear resonant peak is still off by the 1.17% frequency error from Table 16.9 but the lean of the peak and damping levels are much closer to the measured result. This is remarkable as the nonlinear models were fit at a substructure level, yet the predictions at the assembled level seem to represent the measured nonlinearity accurately!

In Fig. 16.18 the time history of the modal acceleration for the first mode of the modified Brake-Reuss Beam (substructure D) is shown. Here one can observe that early in time the linear model, the nonlinear prediction and the measured data match fairly well. However, the linear model has too little damping and so it overestimates the amplitude of the signal by a factor of approximately 5 late in the time history. In contrast, the nonlinear prediction tracks the measured, modally filtered result very well.

Figure 16.19 shows these amplitude dependent properties of the first and second bending modes obtained using the Hilbert Transform as shown in [1]. In the damping curve for the first bending mode, at an amplitude of about (0.040 $kg^{1/2}$ m/s), the response from the substructuring prediction starts to diverge and under predict the damping when compared to the measured data. This could be due to an error in how the modal Iwan Models were fit for substructure C, but similar effects at high amplitudes have been observed in works by Lacayo et al. [18] so it was suspected this may be due to important modal coupling at high amplitude levels.

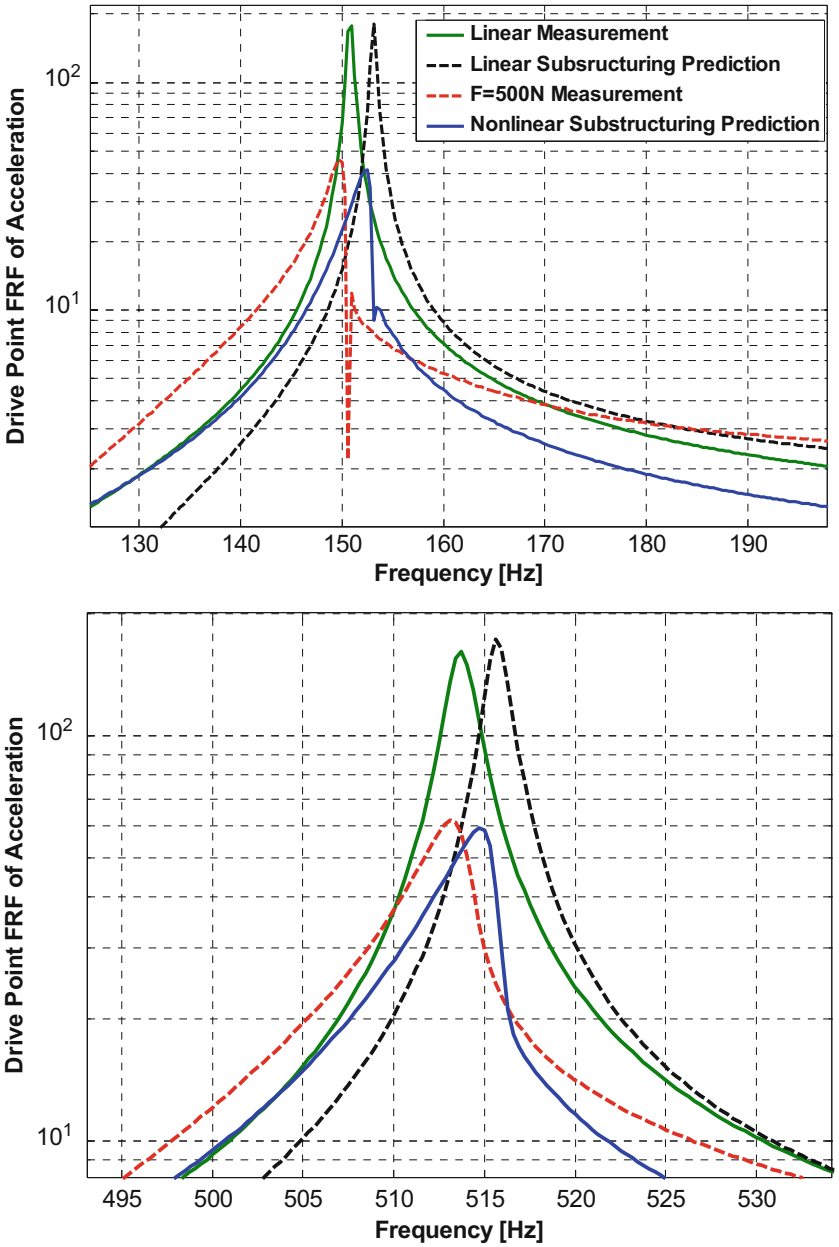

Fig. 16.17 Frequency domain comparison: 1st Bending (*Top*) 2nd Bending (*Bottom*)

Recall from Part I that these models were fit in a least squares sense over several different impulsive loading cases. These loading cases in general were much smaller than the 500 Newtons being tested here. Higher level hits on a substructure level may have led to a model that appropriately fits the damping in a larger range. Another possibility is that the system is reaching the onset of macroslip, and previous studies have shown that nonlinear modal models are accurate only until the onset of macroslip [18]. Therefore if one of the joints is in macro slip, this could lead to erroneous results. Note, for mode 2 the damping seems to match the measured value in the micoslip region and that the offset in the low level damping region is mainly due to inaccuracy in the prediction of the linear damping ratio for this mode.

Using the linear mode shape matrix, the prediction of the modal coordinate response can be transformed into the physical domain and compared to the measured response. Figure 16.20 shows the drive point acceleration obtained using linear substructuring, the nonlinear substructuring prediction and the measured result. As was the case with the individual modes, all three models correlate well very early in time, but the linear model contains insufficient damping and becomes inaccurate later in time. The nonlinear prediction has the correct amplitude over all of the time window.

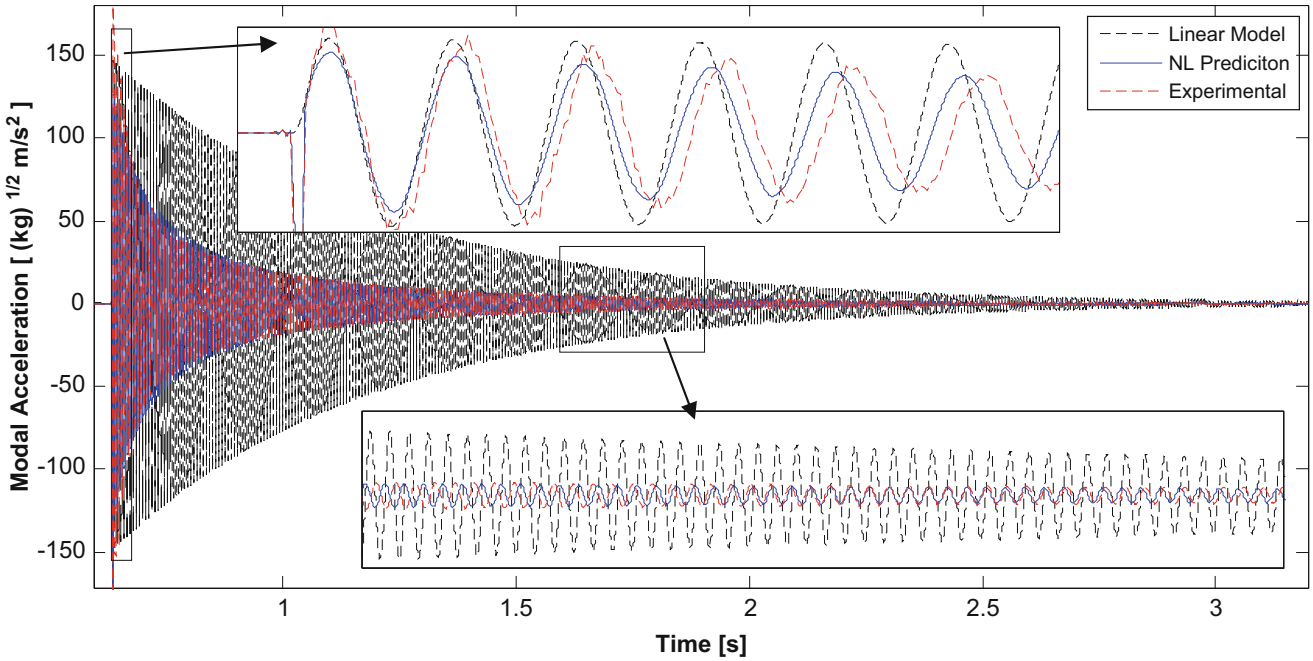

Fig. 16.18 1st Elastic mode: modal acceleration time history

Figure 16.21 removes the linear model from the plot to provide a clearer comparison between the measurement and the nonlinear substructuring prediction. Early in time the nonlinear prediction does a great job capturing the motion of the measured system. Later in time, the shape and amplitude of the curve matches very well with a slight phase shift, due to the frequency error present in the linear substructuring predictions.

16.5 Conclusions

This work utilized uncoupled nonlinear modal models to represent a substructure in a dynamic substructuring problem. These individual components were coupled using the transmission simulator method in order to generate a nonlinear model for the assembly. It is interesting to note that, even though each mode in the original substructure is modeled by an uncoupled, nonlinear single-degree-of-freedom system, the substructuring process spreads the nonlinearity into every mode of the assembled system. As a result, a Newmark integration routine was used to simulate its response to various impulsive loads and thus to compare the amplitude dependent frequency and damping predicted by the model with that measured on a truth model. Each mode of the simulation model and the truth model again behaved as a nonlinear (uncoupled) single-degree-of-freedom system.

Experimental-analytical substructuring predictions were very promising. Linear frequency errors were low (less than 2%) but damping errors were larger (under 50%). The nonlinearity due to the bolted joint caused the damping to change by factors of 6–8; therefore, even though there were relatively large errors in the linear damping ratio predicted by substructuring the effects of the damping nonlinearity were still captured with reasonable accuracy. The nonlinear substructuring results were quite favorable and showed that the substructuring process is quite effective for this system, whose nonlinearity is dominated by micro-slip. The accuracy of the substructured prediction appears to be tied to the accuracy of the modal model used to describe the nonlinear behavior of the structure subcomponents. At high enough amplitudes the authors suspect a significant amount of modal coupling begins to occur, which reveals the main limitation of this methodology.

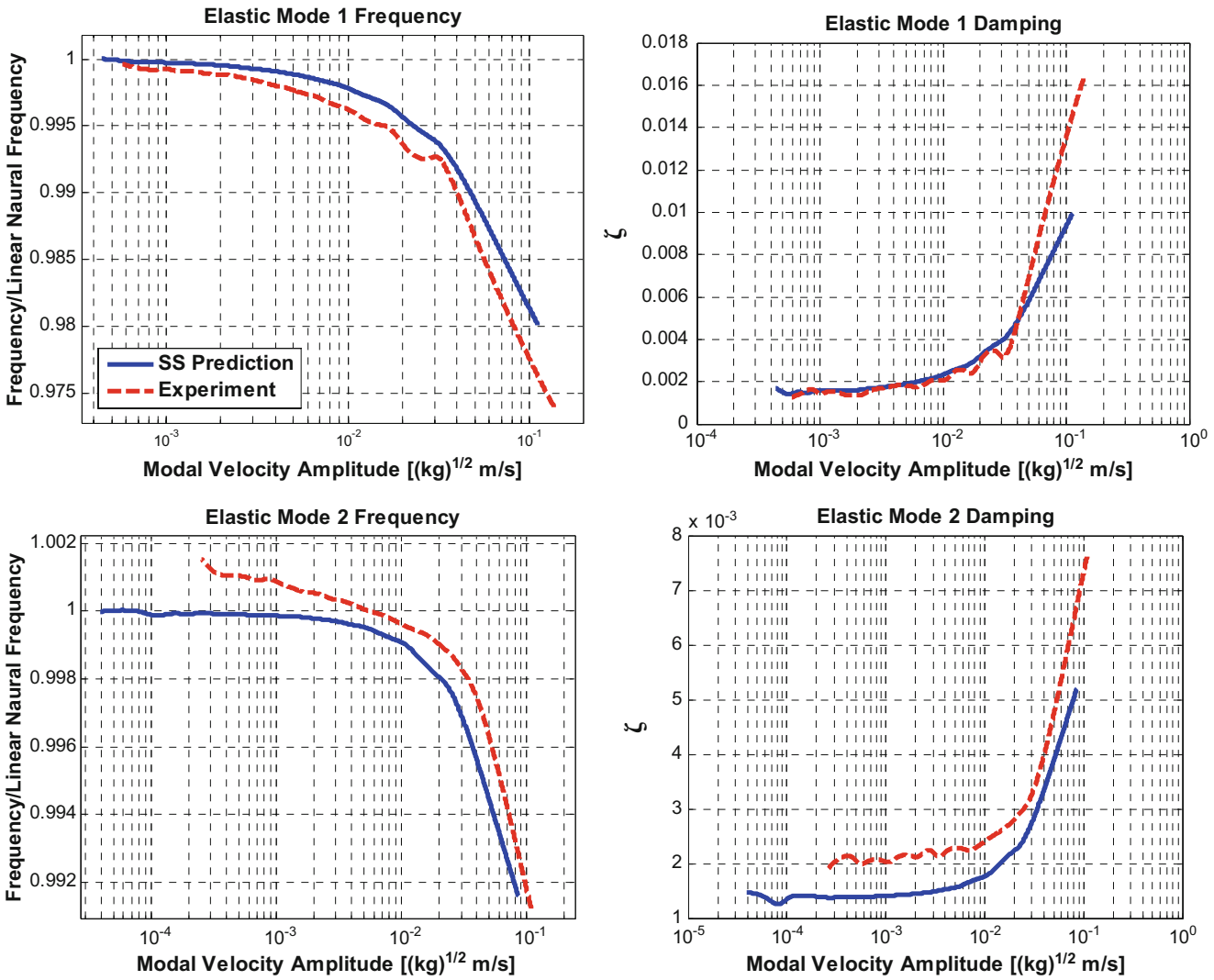

Fig. 16.19 1st and 2nd elastic mode: amplitude dependent stiffness and damping

A FEM model of the beam substructure was also generated for this study. The beam model was updated to linear experimental measurements. Then discrete Iwan parameters were fit to best simulate the nonlinear behavior that was observed in test. This model was used to evaluate the number of sensors needed and their locations as well as to explore the effect of the number of modes retained for each subcomponent. A response prediction based on substructuring with FEM subcomponents was compared to a simulated response from a truth FEM model created by replacing Substructure A with B in the original FEM model. The substructuring predictions from the numerical substructuring suggest that in the absence of experimental noise this nonlinear modal substructuring approach is a quite accurate. In [12] it was tested whether far-field effects and changes on a structure away from the joint change the discrete joint parameters. There the authors used a similar FEM model of the Brake-Reuss Beam. Discrete parameters were fit to match the unmodified system. The FEM was then modified to adjust the far-field structure and these FEM results were compared to test. The results demonstrated (once again when the joints are confined to the microslip regime) that the far-field changes did not significantly change the discrete Iwan parameters that best describe the joints.

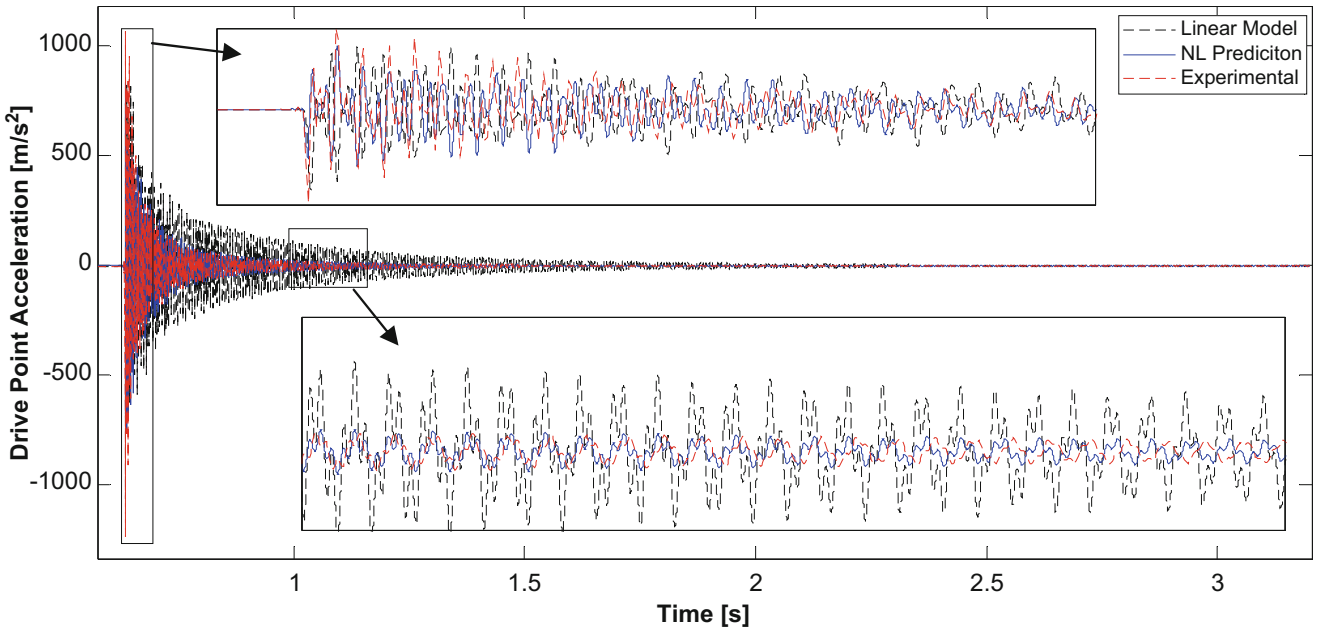

Fig. 16.20 Drive point acceleration for 500 N impulsive load with linear model

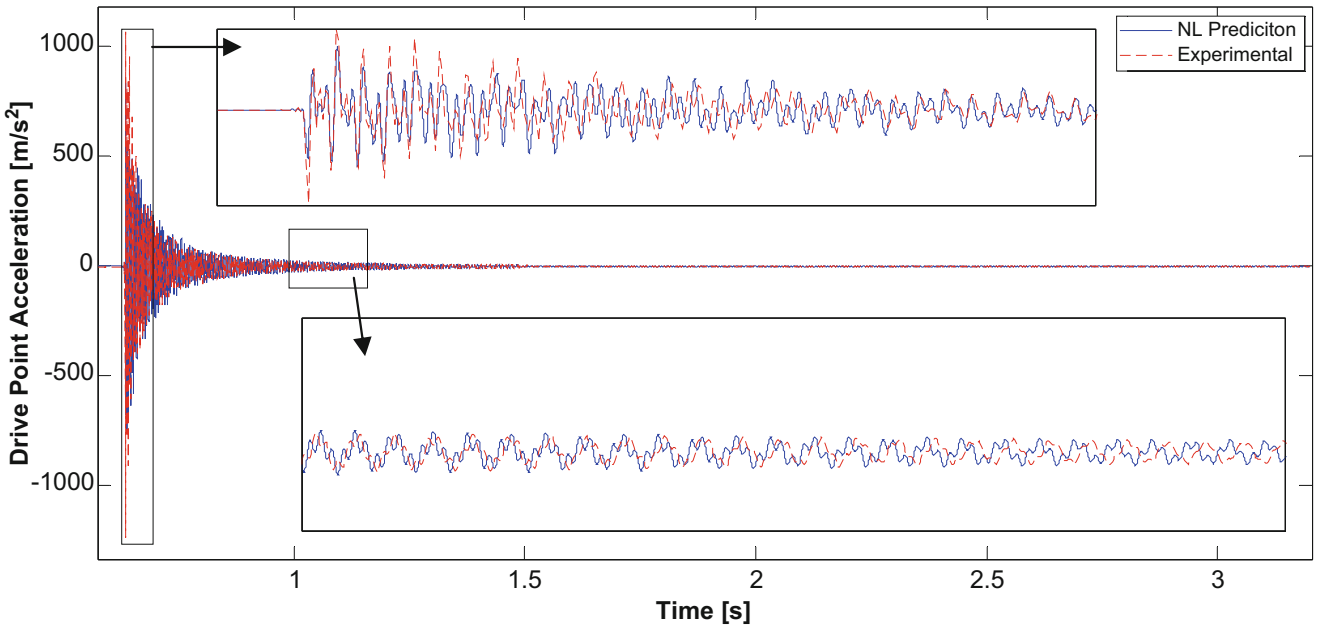

Fig. 16.21 Drive point acceleration for 500 N impulsive load

References

1. Roettgen, D.R., et al.: Substructuring of a nonlinear beam using modal Iwan framework, Part 1: nonlinear modal model identification. Presented at the international modal analysis conference XXXV, Garden Grove, 2017
2. Roettgen, D.R., Allen, M.S.: Nonlinear characterization of a bolted, industrial structure using a modal framework. Mech. Syst. Signal Process. **84**, 152 (2016)
3. Carne T.G., et al.: Force reconstruction using a sum of weighted accelerations technique. Presented at the 10th international modal analysis conference (IMAC X), San Diego, 1992
4. Mayes R.L., et al.: A modal model to simulate typical structural dynamic nonlinearity. Presented at the international modal analysis conference XXXIV, Orlando, 2016

5. de Klerk, D., et al.: General framework for dynamic substructuring: history, review, and classification of techniques. AIAA J. **46**, 1169–1181 (2008)
6. Allen, M.S., et al.: Experimental modal substructuring to couple and uncouple substructures with flexible fixtures and multi-point connections. J. Sound Vib. **329**, 4891–4906 (2010)
7. Mayes, R.L., et al.: Correcting indefinite mass matrices due to substructure uncoupling. J. Sound Vib. **332**, 5856–5866 (2013)
8. Allen, M.S., et al.: Metrics for diagnosing negative mass and stiffness when uncoupling experimental and analytical substructures. J. Sound Vib. **331**, 5435–5448 (2012)
9. Kalaycioglu, T., Ozguven, H.N.: Harmonic response of large engineering structures with nonlinear modifications. Presented at the EURODYN, Leuven, 2011
10. Krack, M., et al.: A method for nonlinear modal analysis and synthesis: application to harmonically forced and self-excited mechanical systems. J. Sound Vib. **332**, 6798–6814 (2013)
11. Allen M.S., et al.: Experimental modal substructuring with nonlinear modal Iwan models to capture nonlinear subcomponent damping. Presented at the international modal analysis conference XXXIV, Orlando, 2016
12. Cooper, S., et al.: Effect of far-field structure on joint properties. Presented at the international modal analysis conference XXXV, Garden Grove, 2016
13. Ginsberg, J.H.: Mechanical and Structural Vibrations, 1st edn. Wiley, New York (2001)
14. Segalman, D.J.: A four-parameter Iwan model for lap-type joints. J. Appl. Mech. **72**, 752–760 (2005)
15. Gross, J., et al.: A numerical round robin for the prediction of the dynamics of jointed structures. Presented at the international modal analysis conference XXXIV, Orlando, 2016
16. Lacayo, R., et al.: Quasi-static modal analysis based on implicit condensation for structures with nonlinear joints. Presented at the international conference on noise and vibration engineering, Leuven, 2016
17. Festjens, H., et al.: Nonlinear model order reduction of jointed structures for dynamic analysis. J. Sound Vib. **333**, 2100–2113 (2014)
18. Lacayo, R., et al.: A numerical study on the limitations of modal Iwan models for impulsive excitations. J. Sound Vib. **390**, 118 (2016)